11-1-2007

AGN REDDENING AND ULTRAVIOLET EXTINCTION CURVES FROM HUBBLE SPACE TELESCOPE SPECTRA

C. Martin Gaskell
University of Nebraska-Lincoln, mgaskell@ucsc.edu

C. Martin Gaskell
University of Nebraska-Lincoln, mgaskell@ucsc.edu

Submitted to Astrophysical Journal
Preprint typeset using LaTeX style emulateapj v. 03/07/07

AGN REDDENING AND ULTRAVIOLET EXTINCTION CURVES FROM HUBBLE SPACE TELESCOPE SPECTRA

C. MARTIN GASKELL[1] AND A. J. BENKER[2]
Department of Physics & Astronomy, University of Nebraska,
Lincoln, NE 68588-0111
Submitted to Astrophysical Journal

ABSTRACT

We present intrinsic extinction curves for 14 AGNs. The AGNs have reddenings, E(B-V), of up to 0.36 mag. The majority (13 out of 14) of the extinction curves are not steep in the UV. Of the seven best determined extinction curves, five have extinction curves that are as flat as the standard Galactic curve in the optical and near UV, but flatter in the far UV, and without the λ2175 feature. One AGN, B3 0754+394, has a steep SMC-like extinction curve, and another, Mrk 304, has an LMC-like extinction curve, including a probable λ2175 bump. The remaining seven, lower-quality, extinction curves have overall shapes that are consistent with an LMC-like shape or a flatter shape. Two have possible λ2175 features, and one might be identical to the Galactic curve. The flatter curves that predominate in our best determined extinction curves are not as flat as the Gaskell et al. (2004) extinction curve for radio-loud AGNs. This suggests that the previous radio-loud extinction curve might be slightly too flat in the range $4 < 1/\lambda < 6.5$ μm^{-1} because of luminosity-dependent reddening biases in the composite spectra, but further investigation is needed. We present a parameterized average AGN extinction curve. Observed variations in the continuum properties of the AGNs are inconsistent with intrinsic object-to-object variations because observed differences are least in the far UV where changes in the accretion disk spectrum should be greatest. We suggest that the steepening of AGN spectra around Lyman α is the result of a small amount of SMC-like dust (E(B-V) ~ 0.03). We find the largest object-to-object differences in spectral shape to be in the Fe II emission of the "small blue bump".

Subject headings: galaxies:active — ISM:dust, extinction - galaxies:quasars:general — black hole physics — accretion: accretion disk

1. INTRODUCTION

Knowing the reddening of the continua and emission lines of AGNs is vitally important for understanding the energy-generation mechanism of AGNs, the physical conditions of the line-emitting gas, the differences between AGNs, and AGN demographics.

Gaskell et al. (2004) showed that reddening is the major cause of differences in optical to UV spectral energy distributions (SEDs), and that the mean extinction in AGNs increases with decreasing luminosity. Gaskell et al. estimated mean AGN extinction curves from composite spectra based on samples of AGNs with different mean extinctions. These extinctions curves differ from the well known extinction curve for dust in the solar neighborhood by lacking the λ2175 carbon feature. The mean extinction curve for the Small Magellanic Cloud (SMC) also lacks the λ2175 feature, but the mean AGN extinction curves found by Gaskell et al. (2004) are considerably flatter than the SMC curve in the ultra-violet. Czerny et al. (2004) also derived a flat extinction curve with no λ2175 bump from SDSS composite AGN colors.

The extinction curves derived by Gaskell et al. (2004) and Czerny et al. (2004) refer to samples of AGNs. Using composite spectra has the advantage of minimizing the effects of possible real differences in the spectral-energy distributions, but the composite spectra necessarily combined quasars of different redshifts. For an apparent-magnitude-limited sample the objects at higher redshift have higher mean luminosities. The luminosity-dependence Gaskell et al. find for the mean extinction therefore introduces the possibility of bias in deriving a extinction curve for AGNs from composite spectra, since the UV part of the extinction curve will tend to come from AGNs with lower mean extinction (Willott 2005). In this paper we avoid this bias by deriving extinction curves for individual AGNs.

The derivation of the extinction curves is discussed in sections 2 and 3, and the curves are presented in section 4. We consider luminosity dependence in section 5 and in section 6 we show that the extinction curves we derive cannot be the result of intrinsic variation of the underlying quasar spectral energy distributions or of varying amounts of host galaxy light. We discuss our results in section 7.

2. SAMPLE

To investigate the shape of the extinction curve one needs carefully calibrated spectra covering the whole ultraviolet and optical spectral regions. Shang et al. (2005) present spectrophotometry of 17 AGNs taken with the *Far Ultraviolet Spectroscopic Explorer (FUSE)* satellite, the *Hubble Space Telescope (HST)*, and the 2.1-m telescope at Kitt Peak National Observatory. The spectra cover rest-frame wavelengths of 900 to 9000Å and are thus well suited for studying reddening. Full observa-

Electronic address: gaskell@astro.as.utexas.edu
[1] Present address: Astronomy Department, University of Texas, Austin, TX 78712-0259
[2] Present address: Department of Physics & Astronomy, University of California, Irvine, CA 92697-4575

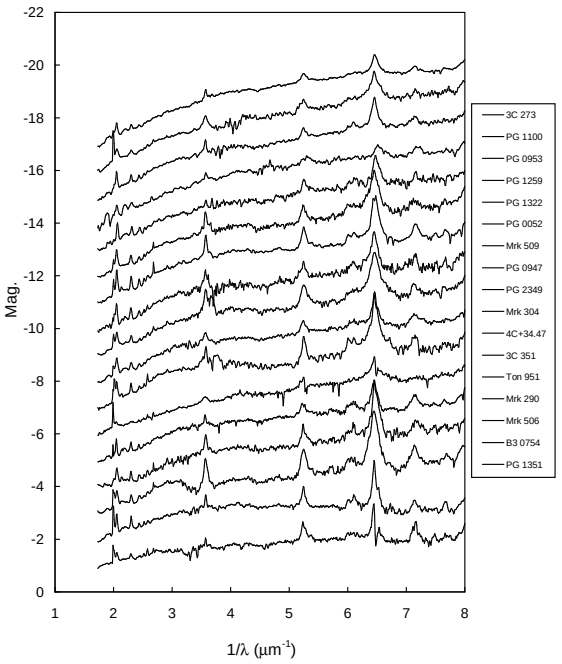

FIG. 1.— Spectra of the FUSE/HST sample. Spectra are shown in F_λ magnitudes normalized to 1.8 μm^{-1}. Spectra have been progressively offset by -1 mag to avoid overlap. Data from Sheng et al. (2005).

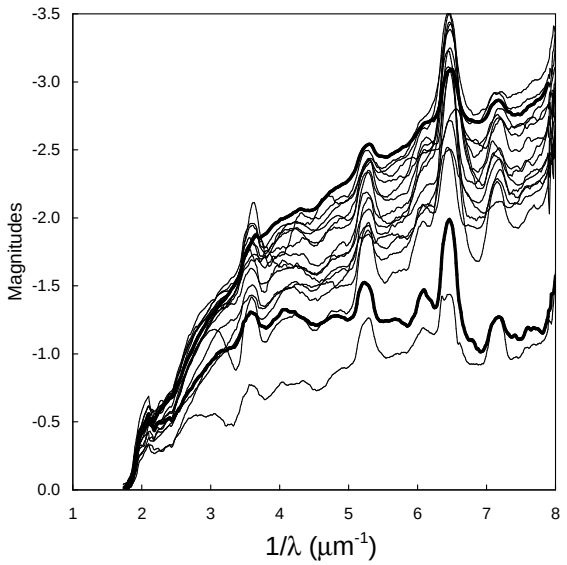

FIG. 2.— Superimposed spectra of the FUSE/HST/optical sample. Spectra are shown in magnitudes normalized to 1.8 μm^{-1}. The spectra have been smoothed to make it easier for the eye to follow individual spectra. The upper of the two thicker lines is 3C 273 and the lower is B3 0754+394. Data from Sheng et al. (2005).

tional details can be found in Shang et al. (2005).

It is important to note that though the Shang et al. sample has the necessary wavelength coverage for determining reddenings, it is a very biased sample. The objects were specifically chosen with the hope that they would be bright in the far-UV (Kriss 2000). This is going to bias the sample in favor of low-reddening AGNs. Nonetheless, we shall see below that quite a number of the AGNs have substantial reddening.

We show all the spectra used in Fig. 1. We do not consider the spectral region shortwards of Lyman α because most of the AGNs show absorption lines in this region (see Fig. 1 of Shang et al. 2005). All spectra have been normalized to the same zero point at 1.8 μm^{-1} and corrected for Galactic reddening. To show the diversity of shapes better we show smoothed versions of the spectra in Fig. 2 without the offsets. Note that the smoothing is purely to reduce confusion for the eye in following individual spectra in this figure, and that the smoothed spectra were not used in the analysis.

3. DETERMINING THE EXTINCTION CURVES

As this paper only addresses the intrinsic reddening in the AGNs, we first removed the reddening due to dust in the Milky Way. We used the reddening estimates of Schlegel, Finkbeiner, & Davis (1998) and a standard Milky Way extinction curve as parameterized by Weingartner & Draine (2001).

The standard method for determining extinction curves is to take the difference in magnitudes between a more reddened object and a less reddened object of the same intrinsic spectral shape. This is most commonly done for pairs of hot stars of the same spectral class. Extinction curves are conventionally given relative to the extinction in the V band and normalized so that the difference in the extinction in the B band relative to the V band is one magnitude (i.e., they are normalized to E(B-V) = 1). The scaling factor which the observed magnitude differences relative to the V band needs to be divided by to give the normalized extinction curve is the difference in reddening, E(B-V), between the two objects.

Crenshaw et al. (2001) derived a extinction curve of NGC 3227 by comparing it with NGC 4151, and Crenshaw et al. (2002) did the same for Ark 564 by comparing it with Mrk 493. Since we have many AGNs here, and because theory suggests the possibility of real differences between the intrinsic spectra of different AGNs, we used an average of several AGNs so that the extinction curves were not just reflecting spectral peculiarities in one AGN at one epoch. We choose as our templates the three AGNs that had the highest relative flux from 4 to 8 μm^{-1} compared with their optical fluxes: 3C 273, PG 1100+772, and PG 0953+414. Although it was not a factor in their selection, these three AGNs happen to represent all three main radio classes: 3C 273 is a core-dominated source, PG 1100+772 is lobe dominated, and PG 0953+414 is radio quiet.

The extinction curves in Fig. 1 and Fig. 2 of Gaskell et al. (2004) were normalized to the B and V bands in the standard way, as described above. However, the uncertainties in normalizing the curves to a relatively small region in the optical are amplified considerably by the time one gets to the UV, so we adopted a different approach. The differences between possible extinction curves, such as the standard Galactic curve or the SMC curve, up to 3 μm^{-1} are, for our purposes, very small, so a more reliable procedure is to normalize the curves over the whole region from the V-band to 3 μm^{-1}. Unfortunately, the region around 3 μm^{-1} is in the middle of the strong broad-line region Balmer continuum and Fe II emission making up the long-wavelength side of the "small blue bump" where there are significant object-to-object variations (see Fig. 1). We therefore moved the baseline of our normalization to the region of 3.75 to 4.07 μm^{-1}. By

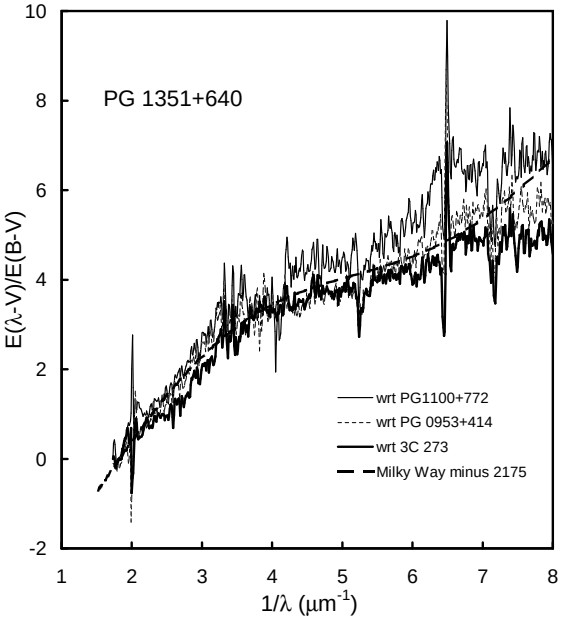

FIG. 3.— Normalized extinction curves for PG 1351+640 derived with respect to the three template blue AGNs. A Milky Way extinction curve with the λ2175 carbon feature removed is shown for comparison.

4 μm^{-1}, known, well-determined extinction curves begin to deviate slightly so we experimented with slightly different normalizations covering the range from SMC extinction curves to the Galactic extinction curve for our local solar neighborhood.

In Fig. 3 we show the differences in the separate extinction curves of one AGN, PG 1351+640, with respect to each of the three separate template blue AGNs. This shows the reader the range of uncertainty caused by using a single template AGN. Note that the differences between the curves would be much smaller had we normalized between 4.5 and 6 μm^{-1}. For the rest of the paper, except where noted, we will just give extinction curves derived with respect to the average of all three template AGNs.

In our extinction curves we have omitted the regions where there are absorption lines. In some spectra there are problems with joining up the UV and the optical (see Shang et al. 2005), and the signal-to-noise ratio is generally worst in these regions. In addition, as can be seen in Fig. 3, matches are poorest around the strong emission lines. We identified three problems in the region of the strong UV emission lines. First, the equivalent widths of the strong emission UV lines in AGNs decrease with increasing luminosity – the well-known "Baldwin effect" (Baldwin 1977, Baldwin et al. 1978) – so to determine reddenings from the emission lines one would have to match AGNs in luminosity. The second problem is that strengths of the cores of the lines also vary with the so-called "eigenvector 1" (EV1, Boroson & Green 1992), so to determine line reddenings one would also have to match AGNs in EV1. The third problem is that the profiles of the UV lines differ from object to object because of the blueshifting of the high-ionization lines (Gaskell 1982). All three of these effects occur to some degree in the AGNs we consider. Since we are confining ourselves in this paper to the issue of the shape of quasar extinction curves, in the majority of cases we have simply deleted the parts of our extinction curves around the major UV emission lines.

TABLE 1
ESTIMATED REDDENINGS FOR AGNS

Object	E(B-V)$_{\lambda 2500}$	E(B-V)$_{\lambda 1700}$	E(B-V)$_{average}$
3C 273	0.000	0.006	0.003
3C 351	0.186	0.150	0.168
4C+34.47	0.094	0.101	0.098
B3 0754+394	0.157	—	0.157
Mrk 290	0.166	0.150	0.158
Mrk 304	0.095	0.120	0.108
Mrk 506	0.234	0.182	0.208
Mrk 509	0.043	0.068	0.056
PG 0052+251	0.032	0.037	0.035
PG 0947+396	0.095	0.094	0.095
PG 0953+414	0.025	0.016	0.021
PG 1100+772	0.013	0.000	0.007
PG 1259+593	0.014	0.036	0.025
PG 1322+659	0.064	0.047	0.055
PG 1351+640	0.366	0.364	0.365
PG 2349-014	0.077	0.082	0.080
Ton 951	0.124	0.155	0.139

4. EXTINCTION CURVES

The process of normalizing the extinction curve for each AGN produces an estimate of E(B-V). We give our E(B-V) estimates in Table 1. Column 2 gives E(B-V)$_{\lambda 2500}$, the reddening from the normalization as described above. Column 3 gives E(B-V)$_{\lambda 1700}$, the reddening obtained by comparing the fluxes in the 4 to 8 μm^{-1} region with the optical flux, and column 4 gives the average of the two estimates. E(B-V)$_{\lambda 2500}$ assumes that the Fe II emission around λ2500 in the small blue bump is the same in all AGNs, while E(B-V)$_{\lambda 1700}$ makes the assumption that all the extinction curves are the same shape. Our method of deriving extinction curves automatically makes the average reddening of our template AGNs zero. In Table 1 we have added a small constant to reddenings of each set to make the reddenings of the bluest template AGN be zero. For the three AGNs with very low reddening (see below), E(B-V)$_{\lambda 2500}$ was found by comparison with 3C 273 alone. The good agreement between E(B-V)$_{\lambda 2500}$ and E(B-V)$_{\lambda 1700}$ suggests that the 1-sigma uncertainty in each E(B-V) estimate is $\pm$0.018 mag, and that the uncertainty in E(B-V)$_{average}$ is $\pm$0.013 mag.

Because the quality of derived extinction curves goes down as the reddening decreases, we present the extinction curves in three groups in order of decreasing reddening and increasing uncertainty. The groups correspond to AGNs with well-determined extinction curves, those with less certain extinction curves, and AGNs with little reddening and hence ill-determined extinction curves.

All extinction curves are known to be smooth in the UV, and, apart from possible λ2175 features, we are only interested in this smooth overall shape. We have therefore, as discussed above, removed the effects of mismatches in the equivalent widths of the strong emission-lines, occasional absorption lines, and, in some cases, the poorer signal-to-noise ratio at the junction between the optical and *HST* observations.

4.1. *Well-Determined Extinction Curves*

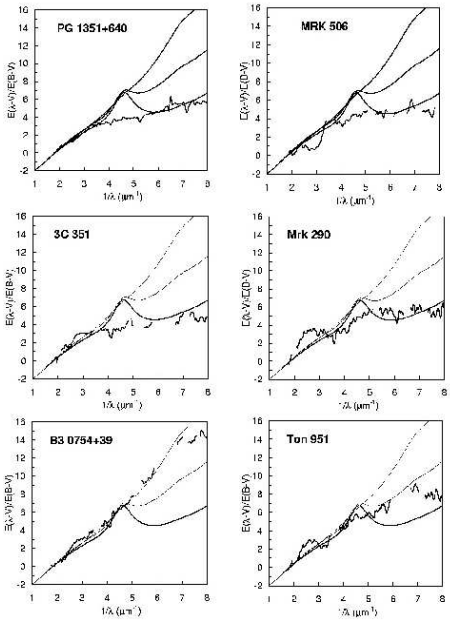

FIG. 4.— Extinction curves, derived using the three template AGNs, for the six AGNs in the sample with the highest extinction. The three smooth curves in each figure are, from top to bottom, the SMC curve, an LMC curve, and the standard Galactic curve for dust in the solar neighborhood.

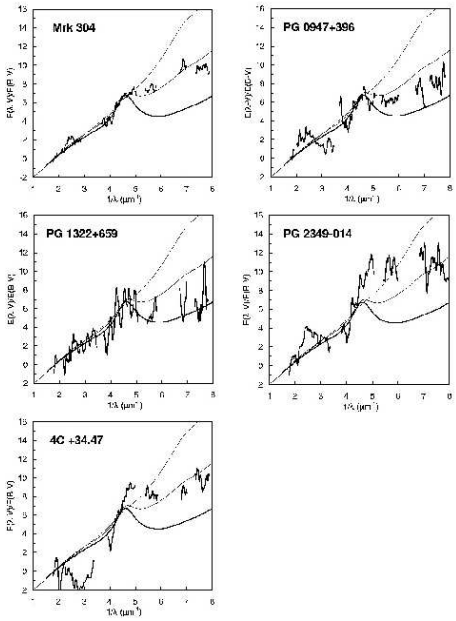

FIG. 5.— Extinction curves for AGNs of lower extinction. As in Fig. 4, these are derived using the three template AGNs. The smooth curves again represent SMC, LMC, and Galactic extinction curves.

In Fig. 4 we show the extinction curves for the six reddest AGNs in the sample. All six lack the λ2175 feature. Only one AGN, B3 0754+394, has an SMC-like curve. Four of the six have curves that are flatter than the Galactic curve in the far UV, and one AGN, Ton 951, is consistent with an LMC-like curve, although, again, it is flatter in the far UV and without the λ2175 feature.

Quasars with low reddening are most sensitive to differences in the spectral shape. These differences are largely due to the broad-line region. Our most heavily-reddened quasar, PG 1351+640 has significant differences in the emission-line strengths and profiles, and also strong absorption (e.g., in C IV), but these differences cause relatively minor differences in the extinction curve (see Fig. 4). One of the well-known differences between AGNs is the strength of the optical and near UV Fe II emission. In the extinction curves one can see the effect of the varying Fe II strength especially on the long-wavelength side of the "small blue bump". This causes the extinction curves around $3\mu\mathrm{m}^{-1}$ to be too high or too low in some objects.

4.2. *Less Certain Extinction Curves*

Fig. 5 shows, in order of decreasing quality, the extinction curves for the five next most reddened AGNs. At lower reddening, the spectral differences mentioned, notably the broad Fe II emission which is not easy to remove, become more important. The best of the curves, that for Mrk 304, is consistent with an LMC-like curve including a probable λ2175 bump. The other four curves are of poorer quality. The extinction curve of PG 1322+659 is quite close to a Galactic extinction curve with a possible λ2175 bump, although the low extinction makes mismatching of emission features a serious problem. PG 0947+396 is consistent with either an LMC-like or a Galactic curve, depending on the normalization. For both PG 0947+396 and PG 1322+659 there is probably a λ2175 bump. The two remaining curves, PG 2349-014 and 4C+34.47, are most consistent with LMC-like curves, but the flatter shape favored by the majority of the AGNs in Fig. 4 is also possible with a different normalization. For 4C+34.47, in addition to the uncertainty in the normalization caused by spectra differences around λ2500, there is an additional uncertainty caused by a gap between the *HST* spectrum and the Kitt Peak spectrum. Inspection of Fig. 1 of Shang et al. (2005) suggests that the optical spectrum could have a slightly too high flux relative to the *HST* spectrum. If this is indeed the case, then the right-hand-side of 4C+34.47 extinction curve (beyond 3.5 $\mu\mathrm{m}^{-1}$) could be lowered by 2–3 magnitudes and it would then resemble the flatter curves in Fig. 4. The reddening, E(B-V), of 4C+34.47 would then be about 0.03–0.04 mag. less than the values in Table 1. The uncertainties in the extinction curves for both 4C+34.47 and PG 2349-014 are too great to say whether λ2175 is present or absent.

4.3. *AGNs With Low Reddening*

For the three AGNs with very low reddening we could not get satisfactory extinction curves using all three template curves, so we only used 3C 273. The three extinction curves in Fig. 6 are shown for completeness and to illustrate that they favor a flatter shape rather than a steep SMC-like shape.

4.4. *The Shape of the Far UV Extinction Curve*

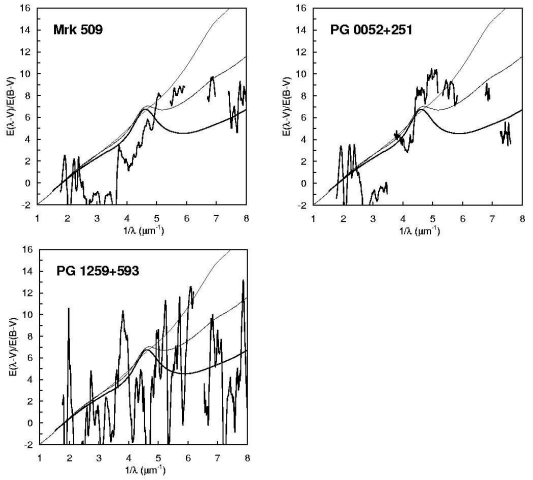

FIG. 6.— Extinction curves for the three AGNs with the lowest extinction. Unlike the curves in the two previous figures, these curves were derived *using only 3C 273 for a template.* The smooth curves represent SMC, LMC, and Galactic extinction curves. We show these curves for completeness and to show that although the extinction curves are noisy, (a) they favor a flatter shape rather than an SMC extinction curve shape and (b) there is no rise in the far UV.

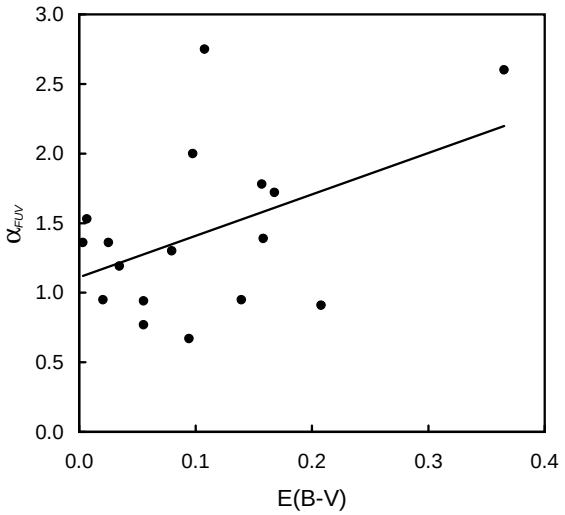

FIG. 7.— The dependence of α_{FUV}, the far ultraviolet spectral index, on the reddening for the AGNs of the *FUSE/HST* sample. The line is least-squares fit.

One can see in Figs. 4, 5 and 6 that, *none* of our curves show a steep rise towards the far UV. Only PG 0947+396 shows a slight rise in the far UV. Even the one SMC-like curve, B3 0754+394, seems to flatten in the far UV. Although we have not derived extinction curves shortwards of Lyman α, it is instructive to look at the correlation of our reddening values with α_{FUV}, the far ultraviolet spectral index in a $F_\nu \propto \nu^{-\alpha}$ power law, measured by Shang et al. (2005) for $\lambda \leq 1100\mathring{A}$. Their α_{UVO}, the slope from 1200–1500$\mathring{A}$, is, as would be expected, well correlated with our reddenings in Table 1 (correlation coefficient, $r = 0.87$ with a one-tailed probability of arising by chance $p < 0.001$). Since α_{UVO} is dominated by reddening, one might therefore expect α_{FUV} to be influenced by reddening too. As can be seen in Fig. 7, while there is a significance correlation ($p = 0.04$) between the reddenings and α_{FUV}, r is only 0.45 (i.e., much less than for the correlation between α_{UVO} and E(B-V).)

The weak dependence of α_{FUV} on E(B-V) supports the idea that, unlike the Galactic curve and the SMC and LMC curves, AGN extinction curves do not rise more steeply into the far UV. This makes physical sense. The rise in far-UV extinction in our Galaxy etc. is the result of a broad spectral feature between 10 and 20 eV that has a similar origin to that of the λ2175 feature (see Fig. 2 of Laor & Draine 1993). Laor & Draine (1993) consider carbon in the form of graphite, but there is also a corresponding spectral feature from PAH molecules (see Li & Draine 2001). Since the majority of our extinction curves lack obvious λ2175, we therefore expect the far UV rise to be absent as well. It is interesting the one curve showing a rise in the far UV, that of PG 0947+396, also shows a possible λ2175 feature.

Although the 10–20 eV peak goes along with the λ2175 bump, the shape of this 10–20 eV feature is much more sensitive to the form the carbon is in and the grain size distribution than the λ2175 feature. Inspection of the *FUSE* composite AGN spectrum of Scott et al. (2004) shows that the sharp peak in the theoretical extinction curve of Weingartner & Draine (2001) due to small graphite grains (see Fig. 9 of Draine 2003) is certainly absent.

The apparently flat far UV extinction curve of AGNs does raise one puzzling issue with the far UV: what is the cause of the turndown in the spectral shape in the far UV? As Shang et al. (2005) show, α_{FUV} is steeper than α_{UVO} by ~ 1. Binette et al. (2005) suggest that this is due to the presence of nanodiamonds in AGN dust. We suggest, however, that perhaps a more natural way of producing this steepening would be by having extinction of E(B-V) ~ 0.03 mag caused by intervening dust with a Galactic, LMC, or SMC extinction curve, as Shang et al. point out. In order not to show up in our extinction curves this dust with a steeper far UV extinction curve would have to be independent of the nuclear dust in the AGN. In agreement with this, our three template AGNs (the rightmost points in Fig. 7) show average α_{FUV} slopes.

4.5. *A Mean Extinction Curve*

It has long been common practice to deredden AGNs with a standard Galactic extinction curve. As we have shown above however, AGN reddening curves differ from the standard Galactic extinction curve by lacking the λ2175 feature and by being flatter in the far UV. In order to provide a better typical AGN extinction curve for de-reddening AGNs we have constructed a mean curve from the extinction curves of the AGNs with the highest reddening, but excluding the SMC-like curve of B3 0754+394. The mean curve was constructed as follows: firstly fourth or fifth order polynomials were fit to the extinction curves of each of the five AGNs through the regions not heavily effected by strong emission lines, and then an unweighted average was then taken of these polynomials. This average extinction curve is shown in Fig. 8 along with the errors in the mean curve. These errors are a minimum around the two regions in which the five input curves were normalized (see section 3). We also show the Galactic extinction curve for the solar neighborhood, and the Galactic extinction curve with the Drude pro-

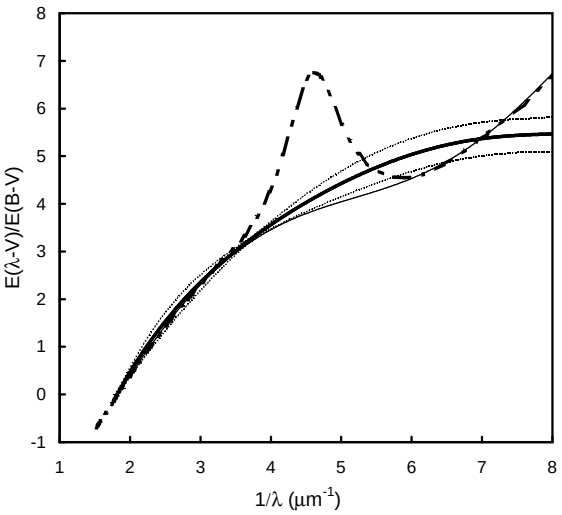

FIG. 8.— The average extinction curve for the five AGNs with greatest reddening (see text). The mean AGN curve is shown as a bold line with 1-sigma error bars for the error in the mean shown as dotted lines on either side of it. The solid dashed-dotted curve is the Galactic extinction curve for the solar neighborhood, and the thin line is the Galactic curve with the λ2175 feature removed.

file of the λ2175 feature removed. As can be seen from Fig 8, the average AGN extinction curve is in excellent agreement with the Galactic curve from the optical up to $\sim 4\mu\mathrm{m}^{-1}$ and possibly to 6 or 7 $\mu\mathrm{m}^{-1}$, but is significantly flatter beyond 7 $\mu\mathrm{m}^{-1}$

For convenience, the mean extinction curve can be represented by a fifth-order polynomial in $x = \lambda^{-1}$ in μm^{-1}, valid over the range $1.5 < x < 8$ (i.e., from Hα λ6564 to Lyman α λ 1216).

$$E(\lambda - V)/E(B - V) = 0.000843x^5 - 0.02496x^4 + 0.2919x^3 - 1.815x^2 + 6.83x - 7.92$$

This equation supersedes the relationships given in the Appendix of Gaskell et al. (2004). For longer wavelengths a standard Galactic extinction curve can be used.

Although the parametrization in Eq.(1) gives a more appropriate extinction curve than assuming that the AGN extinction curve is the same as the Galactic curve, researchers are cautioned that individual AGN extinction curves vary, as can readily be seen in Figs. 4 – 6., so one should, if possible, determine the extinction curve directly for each individual AGN they are studying.

5. LUMINOSITY DEPENDENCE

In Fig. 9 we show the luminosity dependence of our reddenings for the *FUSE/HST* sample compared with the luminosity–mean reddening relationship from Gaskell et al. (2004). As would be expected, given the bias in the *FUSE/HST* sample towards UV-bright objects, the reddenings of the AGNs at a given luminosity mostly lie below the typical values found by Gaskell et al. It can be seen, however, that the two most reddened AGNs for their luminosities have reddenings quite typical of the reddenings in the samples in Fig. 5 of Gaskell et al. (2004).

6. CAN REDDENING BE IMITATED BY DIFFERENCES IN SPECTRAL-ENERGY DISTRIBUTIONS?

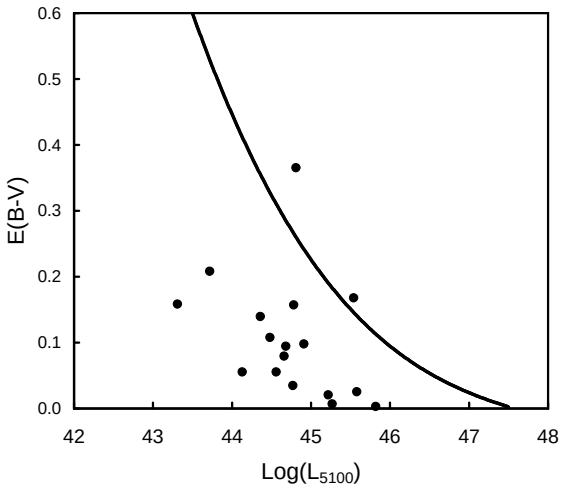

FIG. 9.— The luminosity dependence of the reddenings of the AGNs in the *FUSE/HST* sample. The solid line is from Fig. 5 of Gaskell et al. L_{5100} is λL_λ at λ5100 in ergs s^{-1} from Shang et al. (2005).

With some notable exceptions (e.g., Carleton et al. 1987) it has long been widely considered that apparent differences in AGN spectral energy distributions (SEDs) are caused by intrinsic differences. For example, Yip et al. (2004) concluded from their eigenspectral analysis of a very large sample of SDSS quasars that the spectral differences are primarily due to intrinsic differences in the AGN spectral energy distribution and to varying amounts of host galaxy light. In this section we quantitatively explore these effects and show that they cannot reproduce our observed reddening curves.

Winkler et al. (1992) find no evidence that the *optical* spectrum changes its shape in an individual AGN as it varies, but Barr, Willis & Wilson (1983), and Clavel et al. (1991) observe a hardening of the UV spectra of some AGNs when they brighten. On the other hand it is notable that in the case of Fairall 9 the UV continuum slope stayed the same at $\alpha_{UV} = 0.46 \pm 0.11$ while the UV flux changed by a factor of over 20 (Clavel et al. 1989). We will model possible spectral shape changes in two ways: as a varying "big blue bump" contribution, and as a change in the relative contribution of two power-laws.

6.1. *The Effect of Different Big Blue-bump Contributions*

Krolik et al. (1991) suggest that the luminosity of the "blue bump" varies while an underlying ν^{-1} power-law remains constant. Such variation in an individual object is inconsistent with the optical and IR observations of Winkler et al. (1992), and it is easy to demonstrate that such a variation *between* objects will *not* explain the extinction curves we see.

In the "power law + blue bump" picture, the blue bump is of a thermal origin and has an exponential Wien cutoff. We approximated the bump as a single black body and added an arbitrary $F_\nu \propto \nu^{-1}$ power law. We varied the temperature of the black body, and derived pseudo-extinction curves from the resulting spectra. These curves are normalized to E(B-V) = 1 in the standard manner . We show our results in Fig. 10 along with Milky Way and SMC extinction curves.

The SED of AGNs probably peaks in the EUV/soft

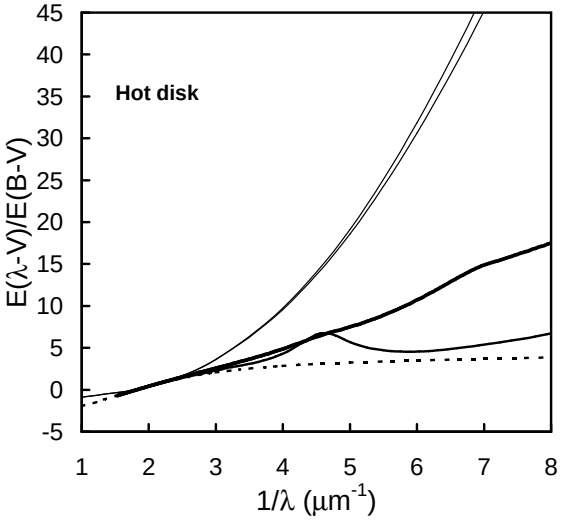

FIG. 10.— Psuedo-extinction curves (thin curves) resulting from a change in the temperature of a hot disk compared with Milky Way (lower thick curve) and SMC (upper thick curve) extinction curves. The top thin curve comes from thermal components of temperatures 300,000K and 200,000K that are 28% and 45% stronger than the power law at Lyman α. The curve just below it is derived from components with similar relative strengths and temperatures of 100,000K and 50,000K. The dotted curve is derived from components of temperatures 300,000K and 200,000K that are 50 times and 80 times stronger than the power law at Lyman α.

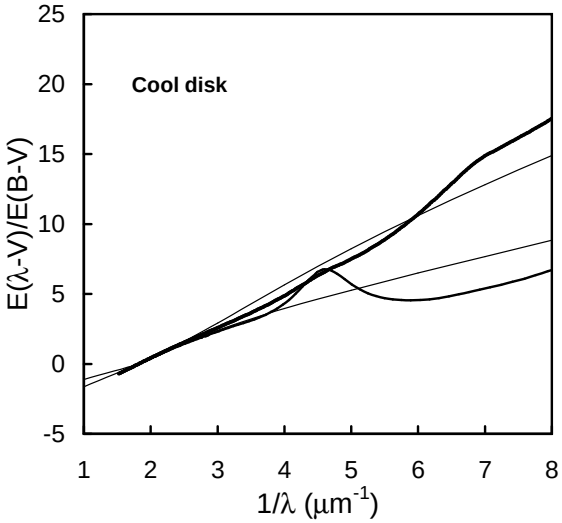

FIG. 11.— Psuedo-extinction curves (thin curves) resulting from a change in the temperature of a cool disk. The thick lines are Milky Way and SMC curves as in Fig. 10. Both of the thin curves come from comparing thermal components of temperatures 40,000K and 20,000K. For the upper curve the thermal components are 37% and nine times stronger than the power law at Lyman α. For the lower thin curve they are 5 times and 37 times stronger than the power law at Lyman α. The top and bottom curves correspond to E(B-V) = 0.098 and 0.175 mag respectively.

X-ray region of the spectrum (see Gaskell, Klimek & Nazarova 2007). This would correspond to temperatures of 100,000 to 300,000 K. We find that the dominant parameter affecting the pseudo-reddening curves is not the temperature or the slope of the arbitrary power law, but the ratio of the thermal component to the arbitrary power law. As can be seen from Fig. 10 the choice of temperature range has little effect on the shape of the pseudo-extinction curves, but varying the ratio of the thermal component to the arbitrary power law has a large effect. The higher the ratio of the thermal component to the arbitrary power law, the flatter the pseudo-extinction curve.

Although it might appear from Fig. 10 that it is easy to produce smooth extinction curves resembling those we have found, this is very misleading. In reality there are two major problems. First, one cannot produce any arbitrary reddening. The largest pseudo reddening produced in Fig. 10 is only E(B-V) = 0.076. Worse still, the pseudo reddening is tied to the shape of the extinction curve. The second major problem is that the shapes of the spectra being compared do not resemble real AGNs. In the *HST* composite of Zheng et al. (1997) the power-law index, α, of the spectral region around Lyman α is 1.72. From the *FUSE* composite of Scott et al. (2004) α = 0.52. For the cases where our pseudo-extinction curves resemble the AGN extinction curves derived above, our thermal component plus arbitrary power law model gives steeply *rising* spectra with $\alpha \approx$ -1.7. Such spectra are never observed.

If we try cooler thermal components with temperatures of around 30,000 K (see Fig. 11) we can only produce SMC- or LMC-like curves. Again, the pseudo-extinction curves depend primarily on the strength of the thermal component relative to the arbitrary power law and are insensitive to the choice of temperatures. It is easier to mimic more significant reddenings. However, the spectral shape problem remains. The 40,000K black body plus power law produces gives a rising spectrum of $\alpha \approx$ -0.5 in the spectral region around Lyman α. This is again at variance with observations.

6.2. *Two Power Laws?*

We also considered an arbitrary mixture of power-laws. The overall optical to X-ray spectral shape of most AGNs can be described with an $\alpha = 1.7$ power law. Winkler et al. (1992) present the shapes of the variable continua for many AGNs. We took the bluest of these to represent the unreddened variable continuum and represent this with an α = -0.2 power law. In Fig. 12 we show the pseudo-extinction curves obtained by adding increasing amounts of the α = -0.2 power law to the $\alpha = 1.7$ power law. The precise choice of spectral indices of the two components is not important. As can be seen from Fig. 12, it is possible to reproduce SMC- or LMC-like curves and somewhat higher apparent reddenings, but the same problems exist as with the thermal components in Fig. 11: the shape of the extinction curve is coupled to the degree of reddening (see caption to Fig. 11), it is not possible to get very high reddenings, and for all but the most modest reddenings, the shapes of the bluest spectra are again much steeper than is observed. In Fig. 13 we show the continuum spectral indices around Lyman α for the bluest spectra as a function of the pseudo reddening.

6.3. *The Effect of Differing Host Galaxy Contributions*

The final effect we consider is the idea that the differences in spectral energy distributions are due to changing host galaxy contributions (Yip et al. 2004). We used a simple cool black body to approximate the effect of a changing host galaxy stellar population and approximated the quasar continuum as a ν^{-1} power law. As is to be expected, all the changes are in the long wave-

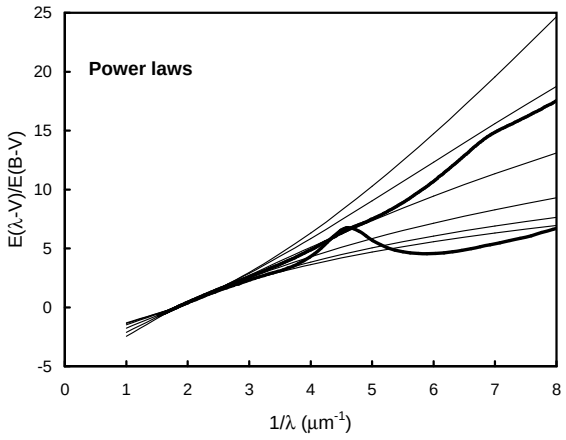

FIG. 12.— Psuedo-extinction curves (thin curves) resulting from adding varying amounts of an α = -0.2 power law to an α = 1.7 power law. The thick lines are Milky Way and SMC curves as in Figs. 10 and 11. The thin lines correspond to effective reddenings of E(B-V) = 0.02, 0.05, 0.13, 0.25, 0.36, & 0.43 magnitudes.

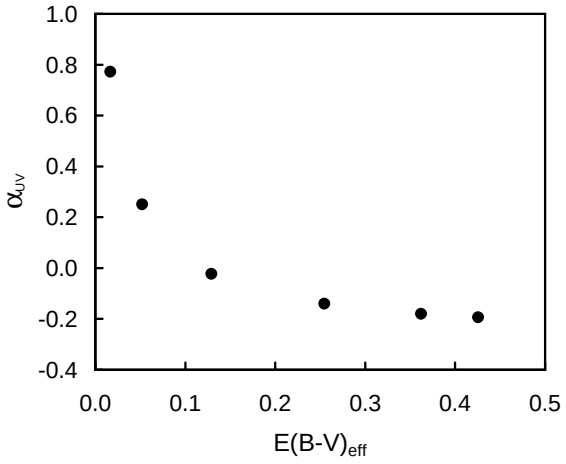

FIG. 13.— Continuum spectral index in the Lyman α spectral region for the bluest AGNs as a function of the pseudo reddening, $E(B\text{-}V)_{eff}$.

length end of the spectrum, and if the changes in spectral shape are interpreted as a pseudo-extinction curve (see Fig. 14), the UV part of the curve bears no resemblance to a reddening curve at all.

From the analysis presented in this section we conclude that changes in the continuum shape from AGN to AGN, either because of changes in the AGN itself or in the degree of host galaxy contamination, are *not* the cause of the extinction curves we have derived. This conclusion is also supported by the similarity of broad-line and continuum reddenings, and reddenings derived from X-rays (see discussion in section 7.6). A positive conclusion that can be drawn from the analysis of sections 6.1 and 6.2, however, is that because changes in continuum shape do mimic reddening to some degree, small changes in the shape of the continua from object to object, if such changes exist, will not be significantly distorting the shapes we derive.

7. DISCUSSION

7.1. *The Fraction of Steep Curves*

Richards et al. (2003) only consider the possibility of AGNs being reddening by SMC-like dust, and Willott

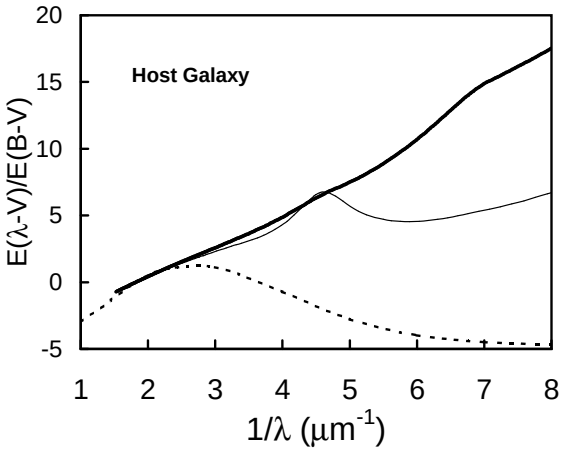

FIG. 14.— Similar to Figs. 11 and 12, but showing the effect of a cooler black body changing its temperature from 4000 to 5000 K (i.e., the range of effective temperature of an old stellar population), and its contribution to the flux at 5500$\AA$ from 19% to 72% compared with a $\alpha = -1$ power law.

(2005) also argues for AGNs being reddened by SMC-like dust, but in our study we find only one clear case of a steep, SMC-like reddening curve, B3 0754+394. We believe the paucity of SMC-like curves is supported by other studies. Gaskell et al. (2004) found quite flat extinction in the UV for the samples of AGNs they considered, especially the radio-loud AGNs. Crenshaw et al. (2001) found a clearly steep, SMC-like extinction curve for the radio-quiet Seyfert NGC 3227 (E(B-V) $\approx$ 0.180 compared with NGC 4151). However, the extinction curve Crenshaw et al. (2002) found for Ark 564 is similar to a number of those in Figs. 4 and 5. Gaskell, Klimek, & Nazarova (2007) find an extinction curve for NGC 5548 similar to our average curve presented here.

Richards et al. (2003) only consider SMC-like reddening curves. Gaskell et al. (2004) have pointed out that the statement by Richards et al. that attempting to explain their large color-segregated composites with reddening "results in good matches at both 1700 and 4040 Å but overpredicts the flux between these two wavelengths and underpredicts the flux shortward of C IV" shows that the reddening curve for the AGNs they consider must in fact be flatter than an SMC-like curve.

As noted in section 2, the FUSE/HST/optical sample of Shang et al. (2005) is biased towards AGNs with low reddening. More specifically, it is biased towards AGNs with low *ultraviolet* reddening. It will therefore be particularly biased against AGNs which are reddened by SMC-like extinction curves. We therefore predict that a less biased sample would not only have more AGNs with higher reddening, but could also have more with steeper (e.g., SMC-like) extinction curves. However, the small spread in the UV slope of AGNs (Cheng, Gaskell, & Koratkar 1991) suggests that steep, SMC-like curves are not common.

7.2. *The λ2175 Feature*

The λ2175 feature has long been known to be weak in AGNs (McKee & Petrosian 1974). Of the six highest quality extinction curves presented here (see Fig. 4), none show the λ2175 feature, while there is an indication that three of the next highest quality five extinction curves might show it. Nonetheless we believe that the λ2175 fea-

ture is relatively rare in AGN extinction curves because it is completely absent in the extinction curves presented by Czerny et al. (2004) and Gaskell et al. (2004) based on composite spectra. Although, as noted in the introduction, luminosity biases can make extinction curves from composite spectra (e.g., those of Gaskell et al. 2004, and Czerny et al. 2004) flatter in the UV than they ought to be (Willott 2005), one thing this will *not* do is affect the strength of λ2175.

7.3. *Emission-line Reddenings*

Emission-line reddenings can be estimated from known line ratios. The He II λ1640/λ4686 and O I λ1304/λ8446 ratios are particularly useful. For Mrk 290 the redshift is low enough that O I λ8446 was observed, and the optical Fe II emission is weak enough that He II λ4686 can be measured. Relative line strengths were estimated by profile fitting. We fit the He II lines with the C IV profile and the O I lines with the Hα profile. We estimate that the line ratios are uncertain by up to about 50%. This is because the lines are weak and determining the appropriate underlying continuum in the presence of other weak lines and the wings of stronger lines is difficult. For Mrk 290 we estimate the He II λ1640/λ4686 ratio to be 3.8. If the real ratio is 8.3, as suggested by photoionization models, then our average extinction curve implies a total reddening, E(B-V) of 0.20, or an intrinsic reddening of 0.18 after allowance for Galactic reddening of 0.016 mag. We estimate the O I λ1304/λ8446 ratio to be 3.1 compared with the theoretical value of 6.5. This implies an intrinsic reddening of 0.17 mag.

These two reddening estimates are in agreement with our estimate of 0.16 mag from the continuum shape (i.e., the value in Table 1). The errors in the reddenings estimated from the O I and He II ratios could be up to $\pm$0.1 mag, but the agreement provides support for the differences in observed continuum shapes being due to reddening. Further careful study of these line ratios in more AGNs would be very worthwhile to check what the zero-point of the reddening is (i.e., what the reddening is for our template AGNs).

7.4. *The Shape of the Spectral-Energy Distribution*

Emission lines provide additional support for our contention that apparent differences in the optical-UV spectral shape are first and foremost due to reddening. We have shown that reddening, and hence the apparent optical to UV spectral index, is luminosity dependent (see Gaskell et al. 2004 and section 9 above). There is no doubt that broad emission lines are produced by photoionization resulting from an ionizing continuum that is an extrapolation of the observed UV-optical continuum. If the UV-optical continuum really were steeper at lower luminosities, rather than being reddened more, then there would be far fewer ionizing photons on average in lower-luminosity AGNs. This would result in much lower emission-line equivalent widths in lower-luminosity AGNs, which is completely the opposite of the Baldwin effect.

With the possible exception of the far UV (see section 4.4), in the spectral region we consider, the only spectral differences we detect that are clearly not due to reddening are due to differing broad-line region properties. These include differing strengths and widths of the major emission lines, and differences in the "small blue bump" due to Balmer continuum and Fe II emission.

7.5. *Implications of Flat Versus Steep Reddening Curves*

The shape of the reddening curve strongly affects the estimated extinction. For a given extinction at λ1640, say, a flat curve such as that in Fig. 8 implies an E(B-V) about three times greater than what an SMC curve would imply. This means that by assuming an SMC-like curve *a priori*, Richards et al. (2003) are underestimating the reddening of SDSS AGNs (e.g., in their Fig. 6) by a factor of 3–5 at higher redshifts.

The larger grain sizes producing the flatter cure could also mean that the ratio, R, of V-band extinction, A_V, to E(B-V) is greater than the value of 3.1 commonly found in the local ISM. Gaskell et al. (2004) suggest that $R \approx 5$ is appropriate for their flat extinction curve.

Taken together, the increased E(B-V) and, to a lesser extent, the possibility of an increased R, means that A_V is a lot greater with a flatter extinction curve than with an SMC-like curve. This has important implications for AGN energetics and demographics.

7.6. *The Amount of Reddening of AGNs*

De Zotti & Gaskell (1985) find, from considerations of broad-band optical colors and Balmer decrements as a function of orientation, that the typical reddening for a large sample of optically-selected Seyfert 1 galaxies is ~ 0.30 mag. Winkler et al. (1992) derive reddenings for a large sample of southern Seyferts from Balmer decrements, the X-ray to Hβ ratio, and variability colors. The mean reddenings from their three methods are E(B-V) = 0.32, 0.41, and 0.29. From a variety of broad-line ratios Ward & Morris (1984) get E(B-V) = 0.27 mag. for NGC 3783. Estimates of the reddening from the UV/optical continuum shapes of individual AGNs are consistent with these reddenings. For NGC 3227 Crenshaw et al. (2001) get E(B-V) = 0.18 relative to NGC 4151, and for Ark 564 Crenshaw et al. (2002) get E(B-V) = 0.14 compared with Mrk 493. For NGC 5548 Gaskell et al. (2005) get E(B-V) = 0.20 compared with 3C 273. All of these AGNs were optically selected. Considering all of these reddening estimates we see that, as expected, the reddenings of the FUSE/HST/optical sample are lower than average for AGNs.

When one looks at complete samples of AGNs selected by radio emission, the reddenings are even greater. For the four increasingly reddened Molonglo samples of Baker & Hunstead (1995) Gaskell et al. (2004) get mean reddenings of E(B-V) = 0.29, 0.34, 0.71, and 0.98 mag. Thus the Baker & Hunstead samples are reddened more than typical optically-selected Seyfert galaxies, and the least reddened of the Molonglo samples is more reddened than the FUSE/HST/optical sample of Shang et al. (2005).

From all these diverse reddening estimates it is difficult to avoid the conclusion that reddening must have a strong effect on the apparent spectral shapes of AGNs. Additional, independent support for steeper slopes being a consequence of dust comes from the correlation between spectral index and the strength of associate absorption (Wills, Shang, & Yuan 2000, Baker et al. 2002).

8. CONCLUSIONS

In agreement with Gaskell et al. (2004) we argue that the UV-optical continuum shape is profoundly affected by reddening for all but the bluest AGNs. We believe that all apparent differences in the UV-optical continua of AGNs are primarily due to differences in extinction and in the forms of the extinction curves. Until the effects of reddening are carefully allowed for it is not possible to investigate possible remaining differences in the spectral energy distributions of AGNs as a function of such things as luminosity, black-hole mass, accretion rate, or radio power. At present all AGNs have optical-UV continuous spectra that appear to be consistent with a single shape after allowance for the effects of reddening and the small blue bump. Even in a sample, such at the *HST/FUSE* sample, biased towards low reddening, most of the objects show detectable reddening.

Our results support the interpretation of Shang et al. (2003) that the second eigenvector in their spectral principal component analysis is due to dust reddening, and disagree with the interpretation of Yip et al. (2004) that the main continuum eigenvectors are due to changing host galaxy contributions and variations in the intrinsic spectral index.

We find rising SMC-like reddening curves to be rare in the relatively low reddening *HST/FUSE* sample we consider and believe that they are not the most common reddening curve for AGNs. Flatter reddening curves imply that the visual extinction of AGNs is greater than if the reddening curves were SMC-like.

We confirm that the $\lambda 2175$ extinction feature is mostly absent in AGN extinction curves. The rise into the far UV seen in the Galactic, LMC, and SMC reddening curves seems also to be mostly absent. These differences imply that the dust has been modified by the AGN environment.

Our new mean AGN extinction curve, while flat in the far UV ($1/\lambda > 6.5\ \mu\mathrm{m}^{-1}$) is steeper in the range $3.5 < 1/\lambda < 6.5\ \mu\mathrm{m}^{-1}$ than the Gaskell et al. (2004) extinction curve from composite spectra of radio-loud AGNs. Although the objects are not the same, the difference suggests that luminosity-dependent extinction (Willott 2005) might have caused the Gaskell et al. curve to be too flat in the UV. In disagreement with Willott (2005), however, we do not find the majority of AGN extinction curves to be SMC-like.

We are grateful to Zhaohui Shang and Mike Brotherton for making the UV and optical spectra available in a convenient form and for useful discussions. We would also like to acknowledge helpful discussions about AGN extinction and related issues with Ski Antonucci and Liz Klimek, and discussion of dust properties with Bruce Draine and Joe Weingartner. We are grateful to Daniel Gaskell for assistance with writing software. This research has been supported by the University of Nebraska UCARE program, by the National Science Foundation through grant AST 03-07912, and by the Space Telescope Science Institute through grant AR-09926.01.

REFERENCES

Baker, J. C., & Hunstead, R. W. 1995, ApJ, 452, L95 (errata 461, L59 [1996a]; 468, L131 [1996b])
Baker, J. C., Hunstead, R. W., Athreya, R. M., Barthel, P. D., de Silva, E., Lehnert, M. D., Saunders, R. D. E. 2002, ApJ, 568, 592
Baldwin, J. A. 1977, ApJ, 214, 679
Baldwin, J. A., Burke, W. L., Gaskell, C. M., & Wampler, E. J. 1978, Nature, 273, 431
Barr, P., Willis, A. J. & Wilson, R. 1983, MNRAS, 202, 453
Binette, L., Magris C., G., Krongold, Y., Morisset, C., Haro-Corzo, S., de Diego, J. A., Mutschke, H., & Andersen, A. C. 2005, ApJ, 631, 661
Boroson, T. A., & Green, R. F. 1992, ApJS, 80, 109
Carleton, N. P., Elvis, M., Fabbiano, G., Willner, S. P., Lawrence, A., & Ward, M. J. 1987, ApJ, 318, 595
Cheng, F. H., Gaskell, C. M., & Koratkar, A. P. 1991, ApJ, 370, 487
Clavel, J., Wamsteker, W., & Glass, I. S. 1989, ApJ, 337, 236
Clavel, J. et al. 1991, ApJ, 366, 68
Constantin, A., & Shields, J. C. 2003, PASP, 115, 592
Crenshaw, D. M., Kraemer, S. B., Bruhweiler, F. C., & Ruiz, J. R. 2001, ApJ, 555, 633
Crenshaw, D. M., et al. 2002, ApJ, 566, 187
Czerny, B., Li, J., Loska, Z., & Szczerba, R. 2004, MNRAS, 348L, 54
De Zotti, G. & Gaskell C. M. 1985, A&A, 147, 1
Draine, B. T. 2003, ARA&A, 41, 241
Gaskell, C. M. 1982, ApJ, 263, 79
Gaskell, C. M., Goosmann, R. W., Antonucci, R. R. J., & Whysong, D., 2004, ApJ, 616, 147
Gaskell, C. M., Klimek, E. S., & Nazarova, L. S. 2007, ApJ, submitted [astro-ph/0711.1025]
Kriss, G. 2000, in ASP Conf. Ser. 224, Probing the Physics of Active Galactic Nuclei, ed. B. M. Peterson, R. W. Pogge, & R. S. Polidan (San Francisco: ASP), 45
Krolik, J. H., Horne, K., Kallman, T. R., Malkan, M. A., Edelson, R. A., & Kriss, G. A. 1991, ApJ, 371, 541
Laor, A., & Draine, B. T. 1993, ApJ, 402, 441
Li, A. & Draine, B.T. 2001, ApJ 554, 778
McKee C. F., & Petrosian V. 1974, ApJ, 189, 17
Richards, G. T., et al. 2003, AJ, 126, 1131
Risaliti, G., Elvis, M., & Nicastro, F. 2002, ApJ, 571, 234
Schlegel, D. J., Finkbeiner, D. P., & Davis, M. 1998, ApJ, 500, 525
Scott, J., Kriss, G., Brotherton, M., Green, R., Hutchings, J., Shull, J. M., & Zheng, W. 2004, ApJ, 615, 135
Shang, Z.-H. Wills, B. J., Robinson, E. L., Wills, D., Laor, A., Xie, B.-G., & Yuan, J.-T. 2003, ApJ, 586, 52
Shang, Z.-H. et al. 2005, ApJ, 619, 41.
Treister, E. et al. 2004, ApJ 616, 123
Ward, M. J., & Morris, S. L. 1984, MNRAS, 207, 867
Weingartner, J. C., & Draine, B. T. 2001, ApJ, 548, 296
Willott, C. J. 2005, ApJ, 627, L101
Wills, B. J., Shang, Z.-H., & Yuan, J. M. 2000, NewA Rev., 44, 511
Winkler, H., Glass, I. S., van Wyk, F., Marang, F., Spencer Jones, J. H., Buckley, D. A. H., & Sekiguchi, K. 1992, MNRAS, 257, 659
Yip, C. W. et al. 2004, AJ, 128, 2603
Zheng, W., Kriss, G. A., Telfer, R. C., Grimes, J. P., & Davidsen, A. F. 1997, ApJ, 475, 469